1/z renormalization of the mean-field behavior of the dipole-coupled singlet-singlet system HoF_3

Jens Jensen
Niels Bohr Institute, Ørsted Laboratory, Universitetsparken 5, 2100 Copenhagen, Denmark
(Received 14 December 1993)

The two main characteristics of the holmium ions in HoF_3 are that their local electronic properties are dominated by two singlet states lying well below the remaining $4f$ levels, and that the classical dipole coupling is an order of magnitude larger than any other two-ion interactions between the Ho moments. This combination makes the system particularly suitable for testing refinements of the mean-field theory. There are four Ho ions per unit cell and the hyperfine coupled electronic and nuclear moments on the Ho ions order in a ferrimagnetic structure at $T_c=0.53$ K. The corrections to the mean-field behavior of holmium trifluoride, both in the paramagnetic and ferrimagnetic phase, have been calculated to first order in the high-density $1/z$ expansion. The effective medium theory, which includes the effects of the single-site fluctuations, leads to a substantially improved description of the magnetic properties of HoF_3, in comparison with that based on the mean-field approximation.

I. INTRODUCTION

The magnetic properties of HoF_3 have been established experimentally[1-3] in considerable detail, and these experiments were recently interpreted in terms of a mean-field (MF) model by Leask *et al.*[1]—HoF_3 is orthorhombic, and the low symmetry at the Ho sites implies that the $J=8$ ground-state multiplet splits into singlets. In the paramagnetic phase, the energy difference between the two lowest singlets is about 0.7 meV and the dipole matrix-element between the two states is large. The next singlet lies at about 5 meV whereas the remaining ones lie between 10 and 50 meV above the ground state,[4] and this arrangement of the crystal-field levels leads to a very anisotropic susceptibility at low temperatures. The system is close to an Ising system, with the only modification that there are two easy directions, one for each magnetically equivalent pair of Ho ions in a unit cell. The classical dipole coupling between the angular moments is weak, but is nevertheless found to be one order of magnitude stronger than any other interaction between the dipoles. It gives rise to strong correlation effects below 5 K and is responsible for the induced magnetic ordering of the singlet ground-state system at $T_c=0.53$ K. The dipole coupling is however not sufficiently strong to produce an ordering of the isolated electronic system. The ratio between the two-ion coupling and the threshold value required for inducing magnetic ordering of the electronic moments is found to be $R=0.86$. The phase transition occurs only because the hyperfine interaction between the electronic and nuclear moments enhances the effective susceptibility, thus leading to a cooperative ordering of the two systems. Below T_c the ordered moments are along the two easy directions. At low temperatures, HoF_3 may be considered to be a simple singlet-singlet system in which the moments interact like classical dipoles. The dipole-dipole interaction can be calculated accurately from first principles and the magnetic system is fully characterized by only a few parameters. The only complications are that there are four magnetic ions per unit cell, that the hyperfine interaction plays an active role, and that additional two-ion couplings are of some importance.

Although the mean-field theory of Leask *et al.*[1] was able to reproduce many of the observations made in HoF_3, such as the excitation spectrum determined by neutron scattering at 1.6 K, some discrepancies remained. The calculated moment in the zero temperature limit was 16% smaller than that observed, and the comparison between the theoretical and experimental heat capacity was not entirely acceptable. Quadrupole-quadrupole couplings may be of some importance in HoF_3 for explaining the discrepancies, but in this paper we shall concentrate on the corrections to the mean-field theory due to the single-site fluctuations. In Sec. II we recapitulate the results of the high-density $1/z$ expansion for the singlet-singlet model utilizing the effective medium approach.[5] The theory is then extended to cover both the paramagnetic and the ordered case. In Sec. III the theory is applied to HoF_3 and the conclusions are presented in Sec. IV.

II. THE 1/z EXPANSION

We consider a Bravais lattice of N identical singlet-singlet atoms, characterized by the energy separation Δ between the two singlets, and by the dipole matrix elements. In the case of a singlet-singlet system, the x axis may be defined so that only the matrix-elements of J_x are nonzero, and M denotes the (numerical) value of this J_x matrix element between the two states, whereas $+m$ and $-m$ are the matrix elements of J_x within, respectively, the lower and upper singlet. $M_0^2=M^2+m^2$ is a constant and $m=0$ in the paramagnetic case at zero field. At the temperature $T=1/k_B\beta$, the MF population factors of the lower and the upper state are n_0 and n_1, where $n_0=1/[1+\exp(-\beta\Delta)]$, $n_0+n_1=1$ and we define $n_{01}=n_0-n_1$.

The two-site Green function is defined as the τ-ordered ensemble average

$$G(ij,\tau_1-\tau_2)=-\langle T_\tau \tilde{J}_{ix}(\tau_1)\tilde{J}_{jx}(\tau_2)\rangle \ . \tag{2.1}$$

$|\tau_1-\tau_2|\leq\beta$, and we use the short-hand notation

$$\tilde{J}_{ix}=J_{ix}-\langle J_x\rangle \ . \tag{2.2}$$

The Fourier transform of the Green function is defined in terms of ($\hbar$ times) the Matsubara frequencies, $\omega_n=2\pi n/\beta$, where n is an integer:

$$G(\mathbf{q},i\omega_n)=\sum_j e^{-i\mathbf{q}\cdot\mathbf{R}_{ij}}\int_0^\beta G(ij,\tau)e^{i\omega_n\tau}d\tau \ . \tag{2.3}$$

The Hamiltonian is divided into two parts, $\mathcal{H}=\mathcal{H}_0+\mathcal{H}_1$, where $\mathcal{H}_0$ is the mean-field part and $\mathcal{H}_1$ is the perturbation

$$\mathcal{H}_1=-\tfrac{1}{2}\sum_{ij}\mathcal{J}(ij)\tilde{J}_{ix}\tilde{J}_{jx} \tag{2.4}$$

in which case the Green function is determined by the linked-cluster expansion

$$G(ij,\tau)=-\frac{\langle T_\tau U(\beta,0)\tilde{J}_{ix}(\tau)\tilde{J}_{jx}(0)\rangle_0}{\langle U(\beta,0)\rangle_0} \tag{2.5}$$

with

$$U(\beta,0)=1-\int_0^\beta \mathcal{H}_1(\tau_1)d\tau_1+\cdots \ . \tag{2.6}$$

The index 0 on the thermal averages indicates that they are the mean-field values. The noninteracting Green function, obtained in the zeroth order of $\mathcal{H}_1$, vanishes if $i\neq j$, whereas if $i=j$ it is

$$G_0(i\omega_n)=-M^2g(i\omega_n)-m^2h(i\omega_n) \ , \tag{2.7}$$

where the two response functions are

$$g(i\omega_n)=\frac{2n_{01}\Delta}{\Delta^2-(i\omega_n)^2} \ , \quad h(i\omega_n)=\beta(1-n_{01}^2)\delta_{n,0} \ . \tag{2.8}$$

The perturbation $\mathcal{H}_1$ cannot, in general, be considered as being small compared to $\mathcal{H}_0$, but each time a term involving the two-ion coupling is summed over $\mathbf{q}$, we effectively gain a factor $1/z$, where z is the coordination number. A systematic expansion of the Green function in powers of $1/z$, in the case of the singlet-singlet system, was developed by Stinchcombe.[6] Here, we shall use a slightly different approach and utilize the concept of an effective medium which is the basis of the coherent-potential approximation.

The ensemble averages in (2.5) are calculated by expressing the angular momentum operators in terms of the "standard-basis" operators, $a_{\nu\mu}=|\nu\rangle\langle\mu|$ where $|\nu\rangle$ are the MF eigenstates of an atom, and by utilizing the invariance of the trace to a cyclic permutation of the operators.[7,8] These are not Bose operators, so the "contractions" determined by the commutators of the different operators are not c numbers, but operators which give rise to new contractions. However, the next generation of contractions adds terms to $G(\mathbf{q},i\omega_n)$ which always involve additional $\mathbf{q}$ summations. Hence in the order $(1/z)^0$, these contractions are neglected. This corresponds to a decoupling of the higher-order cumulants in (2.5) into products of the second-order terms, $\langle T_\tau\tilde{J}_{ix}(\tau_1)\tilde{J}_{jx}(\tau_2)\rangle_0=-\delta_{ij}G_0(\tau_1-\tau_2)$ (if the possible difference between $\langle J_x\rangle$ and $\langle J_x\rangle_0$ is neglected, see below). The infinite series of "chain diagrams," generated by (2.5) using this decoupling, is easily summed, and the result is

$$G(\mathbf{q},i\omega_n)|_{\mathrm{RPA}}=\frac{G_0(i\omega_n)}{1+\mathcal{J}(\mathbf{q})G_0(i\omega_n)} \tag{2.9}$$

showing that this approximation is equivalent to the random-phase approximation (RPA). The difference between the fourth-order cumulant and the corresponding decoupled value appears in the next order of $1/z$. In the usual "unconditional" cumulant expansion this difference, the fourth-order semi-invariant, is introduced as an additional vertex. The vertex in the RPA chain diagrams is replaced by the sum of this and the fourth-order semi-invariant, and neglecting any particular effects of whether some vertices in a chain belong to the same site or not, we may straightforwardly sum the series.[6]

In the order $1/z$ only the single-site Green function is directly modified, as the fourth-order cumulant only differs from the decoupled one if all the four momentum operators belong to the same site. The single-site Green function is

$$G(i\omega_n)\equiv G(ii,i\omega_n)=\frac{1}{N}\sum_q G(\mathbf{q},i\omega_n) \tag{2.10}$$

and, to the order $1/z$, the two-site Green function may be expressed in terms of $G(i\omega_n)$ by introducing the effective-medium coupling

$$K(i\omega_n)=\frac{1}{N}\sum_q \mathcal{J}(\mathbf{q})G(\mathbf{q},i\omega_n)/G(i\omega_n) \tag{2.11}$$

in which case

$$G(\mathbf{q},i\omega_n)=\frac{G(i\omega_n)}{1+\{\mathcal{J}(\mathbf{q})-K(i\omega_n)\}G(i\omega_n)} \ . \tag{2.12}$$

$K(i\omega_n)$ is the sum of all chain diagrams which start and end at the same site without crossing this site in between.[5] We may therefore consider an effective cumulant expansion of $G(i\omega_n)$, equivalent to (2.5) where $\mathcal{J}(ij)$ in $\mathcal{H}_1$ is replaced by the time-dependent coupling $K(\tau_1-\tau_2)$, and the term to leading order in this coupling is

$$-\tfrac{1}{2}\int_0^\beta\int_0^\beta\int_0^\beta d\tau\,d\tau_1 d\tau_2 e^{i\omega_n\tau}\frac{1}{\beta}\sum_{n'}K(i\omega_{n'})e^{i\omega_{n'}(\tau_1-\tau_2)}$$

$$\times[\langle T_\tau\tilde{J}_{ix}(\tau_2)\tilde{J}_{ix}(\tau_1)\tilde{J}_{ix}(\tau)\tilde{J}_{ix}(0)\rangle_0-\langle T_\tau\tilde{J}_{ix}(\tau_2)\tilde{J}_{ix}(\tau_1)\rangle_0\langle T_\tau\tilde{J}_{ix}(\tau)\tilde{J}_{ix}(0)\rangle_0] \ . \tag{2.13}$$

The decoupling of the higher-order cumulants in the single-site series into products of the second-order terms leads to the result

$$G(i\omega_n)|_{\mathrm{RPA}}=\frac{G_0(i\omega_n)}{1+K(i\omega_n)G_0(i\omega_n)} \tag{2.14}$$

and when this result is introduced in (2.12), $K(i\omega_n)$ cancels out and we get the RPA result, (2.9). To the next order in $1/z$ we have to include the fourth-order cumulant term, (2.13). We shall first consider the paramagnetic phase, $m=0$, in which case

$$G(i\omega_n)=G_0(i\omega_n) -G_0(i\omega_n)\{K(i\omega_n)G_0(i\omega_n)+\Sigma(i\omega_n)\}+\cdots , \tag{2.15}$$

where the renormalization factor is

$$\Sigma(i\omega_n)=\alpha+\gamma(i\omega_n)g(i\omega_n) \tag{2.16}$$

α is a constant

$$\alpha=\frac{M^2}{n_{01}^2}[\lambda_2-\tfrac{1}{2}\{g(0)+\beta(1-n_{01}^2)\}\lambda_1] \tag{2.17}$$

and the frequency-dependent term is

$$\gamma(i\omega_n)=\frac{M^2}{n_{01}^2}[\lambda_1-(1-n_{01}^2)K(i\omega_n)] \tag{2.18}$$

and the parameters λ_p are defined as

$$\lambda_p=\frac{1}{\beta}\sum_{n'}K(i\omega_{n'})[g(i\omega_{n'})]^p . \tag{2.19}$$

The unconditional cumulant expansion accounts correctly for the fourth-order cumulant term in (2.15), but an analysis of the sixth and higher-order terms shows that this procedure does not lead to a good estimate of the higher-order contributions in the single-site series. Instead, it is found that the series generated by replacing $G_0(i\omega_n)$ in front of the second term of the single-site series (2.15) by the interacting Green function $G(i\omega_n)$, much more effectively accounts for the terms deriving from specifically, the sixth-order cumulant. Introducing this Dyson-like result for the single-site Green function in (2.12), we get

$$G(\mathbf{q},i\omega_n)=\frac{G_0(i\omega_n)}{1+\Sigma(i\omega_n)+\mathcal{J}(\mathbf{q})G_0(i\omega_n)} \tag{2.20}$$

valid to first order in $1/z$. This result is nearly the same as the one derived by Galili and Zevin[9] using an elaborate renormalization of the unconditional expansion. In addition to the simplifications attained by utilizing the effective-medium approach, the present procedure is fully self-consistent. A more detailed discussion of the effective medium theory and its comparison with the unconditional cumulant expansion may be found in Refs. 5 and 10. In a systematic expansion in $1/z$, the effective-medium approximation ceases to be valid in second order. However, an improvement of the theory is obtainable by including the new diagrams due to the sixth-order cumulants into the single-site series, neglecting the corresponding $(1/z)^2$ two-site effects. The second-order contributions to the effective medium have been considered in an analysis[11] of Pr and are of some importance if the energy gap in the excitation spectrum is small. In the present analysis we shall consider only the leading-order $1/z$ modifications due to the single-site fluctuations.

In the paramagnetic phase, the contribution of the fluctuations to the internal energy is

$$\delta U=\frac{N}{2\beta}\sum_n\left[K(i\omega_n)-\frac{\Delta+i\omega_n}{M^2}\right]G(i\omega_n)-Nn_1\Delta \tag{2.21}$$

and introducing the $1/z$ result for $G(i\omega_n)$ in this expression, we may write the energy change

$$\delta U=\frac{N}{2}\left[\frac{\alpha n_{01}}{1+\alpha}\Delta-M^2\lambda_1 +\frac{1}{\beta}\sum_n K(i\omega_n)\{G(i\omega_n)-G_0(i\omega_n)\}\right] , \tag{2.22}$$

where the last sum is a small second-order term. The derivative of δU with respect to T determines the change of the heat capacity from its mean-field value. In the calculation of the energy it is of importance that the Green function satisfies the sum rule:

$$\frac{1}{\beta}\sum_n G(i\omega_n)=-M^2 \tag{2.23}$$

($m=0$). This is strictly the case if the single-site series is terminated after the first or the second term in (2.15). It is also found numerically to be valid with a rather high accuracy for the self-consistent $1/z$-Green function.

Next we wish to consider the situation when $m\neq 0$. In the low-temperature regime, with which we shall mostly be concerned, the elastic pole in (2.7) is weak compared to the inelastic one, unless the system is close to the saturation limit $m\gg M$. However, in this limit, i.e., at high fields, all the fluctuations are quenched and the mean-field approximation is valid. This means that, generally, at low temperature the elastic fluctuations are of less importance than the inelastic ones, and it is therefore acceptable to include the elastic-pole contributions less rigorously.

The first problem we meet in the order $1/z$ is that, if we define the mean-field Hamiltonian in the usual way, $\langle\tilde{J}_x\rangle_0$ will in general be nonzero, giving rise to additional complications in the linked-cluster expansion of the Green function. In order to avoid these complications we introduce a modified mean field, H_{MF}, defined by the requirement that

$$\langle J_x\rangle=\langle J_x\rangle_0=m^2n_{01} \tag{2.24}$$

which differs from the usual mean field H_0:

$$H_{\mathrm{MF}}=H_0-\delta H;\quad g\mu_BH_0=g\mu_BH+\mathcal{J}(0)\langle J_x\rangle , \tag{2.25}$$

where H is the applied field. The determination of $\mathcal{H}_0$ in terms of H_{MF} instead of H_0 introduces an extra perturba-

tion in the Hamiltonian, $\mathcal{H}=\mathcal{H}_0+\mathcal{H}_1+\mathcal{H}_2$, with $\mathcal{H}_2=-g\mu_B\delta H\sum_i \tilde{J}_{xi}$. The ratio $\delta H/H_{\rm MF}$ is a small quantity, at the most about 0.1 in the numerical calculations, and $\mathcal{H}_2$ is truly a weak perturbation. Furthermore, the leading order modification of the cumulant expansion is proportional to $(\delta H/H_{\rm MF})^2$, which small correction is neglected.

The elastic pole disturbs the inelastic fluctuations, and $\Sigma(i\omega_n)$ in (2.20), when $n\neq 0$, is changed into

$$\Sigma(i\omega_n)=\alpha-\alpha_m+\left[\gamma(i\omega_n)-\frac{2m^2}{M^2}\gamma(0)\right]g(i\omega_n) \tag{2.26}$$

with

$$\alpha_m=\frac{m^2}{n_{01}^2}\left[\lambda_2-g(0)\lambda_1+\frac{4}{g(0)}\lambda_3 -(1-n_{01}^2)(1+\tfrac{1}{2}\beta\Delta n_{01})K(0)g(0)\right] . \tag{2.27}$$

In this result we have for simplicity neglected some frequency-dependent terms which vanish in the zero-frequency limit [$g(i\omega_{n'}\pm i\omega_n)$ appearing as a factor in the n' sums has been replaced by its zero-frequency value $g(i\omega_{n'})$]. The inelastic broadening of the elastic peak discussed in Ref. 11 is neglected in this approximation. In addition to the inelastic modifications we get elastic terms appearing only at zero frequency, and at this frequency the single-site Green function is found to be

$$G(0)=-\frac{M^2g(0)}{1+\Sigma(0)-M^2K(0)g(0)}-m^2\xi h(0) , \tag{2.28}$$

where $\Sigma(0)$ is the zero-frequency value of $\Sigma(i\omega_n)$ given by (2.26) and

$$\xi=\frac{1+\tanh[m^2n_{01}^2\beta K(0)-M^2\beta\lambda_1]}{1+[4n_{01}^2K(0)g(0)+2\lambda_2+g(0)\lambda_1]M^2/n_{01}^2} . \tag{2.29}$$

The cumulant expansion of the elastic contribution effectively becomes an expansion in $\beta K(0)$ which converges slowly at low temperatures, where however the elastic term as a whole is frozen out. The actual result for the $1/z$ term in the numerator of ξ, deriving from the fourth-order cumulant, is the leading order term in the Taylor expansion of the tanh term, which diverges in the zero-temperature limit. This divergence was not found to influence the numerical results significantly, as the term is multiplied by $h(0)$ which vanishes exponentially in this limit. However, in order to account in a simple way for the renormalization of this term expected due to higher-order contributions, we have replaced the $1/z$ term by its tanh value.

The final result for $G(\mathbf{q},i\omega_n)$ to first order in $1/z$ when m is nonzero is determined in terms of $G(i\omega_n)$. At nonzero frequencies the result may be written as (2.20), with $\Sigma(i\omega_n)$ now given by (2.26). At zero frequency we have to introduce $G(0)$ given by (2.28) in the original expression (2.12) for $G(\mathbf{q},i\omega_n)$. The result (2.12) becomes equivalent to the RPA result if $G_0(i\omega_n)$ in (2.9) is replaced by the effective noninteracting Green function

$$\tilde{G}_0(i\omega_n)=\frac{G(i\omega_n)}{1-K(i\omega_n)G(i\omega_n)} \tag{2.30}$$

which is equal to $G_0(i\omega_n)/[1+\Sigma(i\omega_n)]$, except in the zero-frequency case when $m\neq 0$.

The mean field $H_{\rm MF}$ is determined by (2.24) which may be written

$$\langle J_x\rangle=\langle J_x\rangle_0=-g\mu_B\int_0^{H_{\rm MF}}G_0(0;H')dH' , \tag{2.31}$$

where $G_0(0;H')$ is the noninteracting Green function, (2.7), as a function of the Zeeman-field H'. Differentiating this equation with respect to the applied field $g\mu_BH$, at a constant temperature, we get on the left-hand side the static bulk susceptibility $-G(\mathbf{0},0)$, or

$$G(\mathbf{0},0;H)=G_0(0;H_{\rm MF})\{1-\mathcal{J}(\mathbf{0})G(\mathbf{0},0;H)\}\frac{dH_{\rm MF}}{dH_0} \tag{2.32}$$

which is directly integrable, as $H_{\rm MF}$ is the mean field determining $G(\mathbf{0},0;H)$, and we get the following relation between the two field quantities

$$H_0=\int_0^{H_{\rm MF}}\frac{G_0(0;H')}{\tilde{G}_0(0;H')}dH' \tag{2.33}$$

making use of the effective noninteracting Green function defined by (2.30). The combination of (2.33) and (2.25) determines the relation between the applied field and the mean field, which allows a fully self-consistent calculation of $\langle J_x\rangle$ as a function of field, in much the same way as in the MF approximation. The adjustment of the mean field, by replacing H_0 by the effective value $H_{\rm MF}$, implies that the change in the free energy including the $1/z$ contributions, relatively to the nonmagnetic state, is determined by the mean-field part of the Hamiltonian, $\mathcal{H}_0$, because $dF/N=-g\mu_B\langle J_x\rangle dH$ is equal to $-g\mu_B\langle J_x\rangle_0 dH$ (at constant temperature). This has the consequence that

$$\delta F(m=0)=-N\int_0^{M_0}g\mu_B\delta H d\langle J_x\rangle . \tag{2.34}$$

M_0 is the saturation value of $\langle J_x\rangle$ in the limit of an infinite field, in which limit any correction to the MF approximation vanishes. The difference $\delta H=H_0-H_{\rm MF}$ is considered to be a function of $\langle J_x\rangle$, and introducing $\delta F(m=0)$, as determined by δU in (2.22) and the corresponding change in heat capacity, the fulfillment of (2.34) provides an independent test of the theory.

III. THE MAGNETIC PROPERTIES OF HoF_3

HoF_3 is orthorhombic with the lattice parameters $a=6.404$ Å^{-1}, $b=6.875$ Å^{-1}, and $c=4.379$ Å^{-1}, and there are 4 Ho^{3+} and 12 F^- ions per unit cell. The positions of the ions within the unit cell are specified in the previous papers[2,3] on HoF_3, and the projections of the ions on the a-c and a-b planes are shown in Fig. 1. The crystal-field Hamiltonian for the Ho ions at the four different sites in the unit cell is the same when referring to one local coordinate system for the sublattices labeled 1 and 2 in Fig. 1 and another, in which the b and c axes

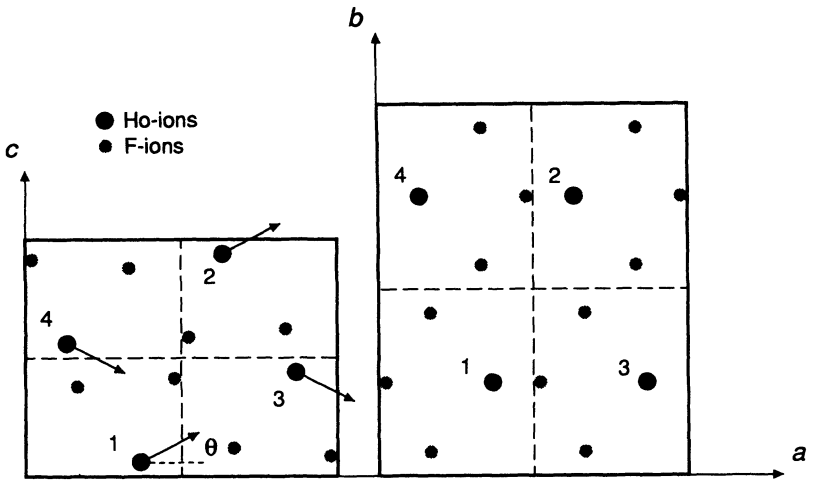

FIG. 1. The 4 Ho and 12 F ions in one unit cell of the orthorhombic structure of HoF_3, projected on the a-c and the a-b plane. The arrows indicate the local x axes lying in the a-c plane and making the angles $\pm\theta$ with the a axis, which are also the directions of the moments in the ordered phase. The figure shows the case where $\theta=+25°$.

are reversed, for the sublattices 3 and 4. The local easy axes, or x axes, are indicated in the figure. They lie in the a-c plane and make the angles θ and $-\theta$ with the a axis. The magnitude of θ, but not its sign, is known from the experiments.[1,2] The sign of θ has not much influence on the analysis, but we have here chosen $\theta=+25°$ as also used in Fig. 1. This choice of sign leads to a slightly better fit of the magnetization curves than the other, but the difference is not so significant that it rules out the alternative choice.

The equivalence of the ions, when considered in their local coordinate systems, makes it straightforward to generalize the theory in the preceding section to this case with four magnetic ions per unit cell. In the paramagnetic phase the only modification of the RPA calculations presented in Ref. 1 are that the components in the single-ion susceptibility tensors $\bar{\bar{\chi}}_r^0(\omega)$, deriving from the singlet-singlet transition on the rth ion, should be divided by the common renormalization factor $1+\Sigma(\omega)$. This follows from the fact that the RPA expression for the final Green function is unchanged if the noninteracting Green function $G_0(i\omega_n)$ in (2.9) is replaced by the effective $\tilde{G}_0(i\omega_n)$ given by (2.30). Neglecting small $1/z$ corrections of the RPA contributions from other single-ion transitions, this procedure allows the full scheme of the ions to be included in the calculations. The imaginary part of $\Sigma(\omega)$ is proportional to the imaginary part of $K(\omega)$ times $(1-n_{01}^2)$, and the latter factor is vanishing small at low temperatures, thus $\Sigma(\omega)$ is real just above T_c. In this limit the paramagnetic density of states, for each of the $4N$ magnetic ions, is

$$\mathcal{N}(\varepsilon)=\frac{1}{4N}\sum_{\mathbf{q},\nu}\delta(\varepsilon_{\mathbf{q},\nu}-\varepsilon)\ , \tag{3.1}$$

where $\varepsilon_{\mathbf{q},\nu}$ are the four excitation energies at a certain $\mathbf{q}$. The $\mathbf{q}$ summation in the expression (2.11) for $K(i\omega_n)$ may be replaced by an energy integration by the introduction of $\mathcal{N}(\varepsilon)$. The resulting integral is the same as the one derived for a Bravais lattice. Calculating $K(i\omega_n)$ in this way, the final density of states has been determined self-consistently by an iterative procedure, using the RPA as a starting point. The result, nominally at 0.55 K, is shown in Fig. 2. The corresponding excitation energies at 1.6 K along the high-symmetry directions $(h00)$ and $(00l)$ are shown in Fig. 3. As discussed in Ref. 1 an effective double-zone representation is applicable along these directions, and only two modes scatter the neutrons in a constant-$\mathbf{q}$ scan. The calculated dispersion relations, the solid lines in Fig. 3, are compared with the experimental neutron-scattering results and the RPA predictions presented in Ref. 1. Although the excitation energies in the order $1/z$ are not changed much compared to the RPA theory, the tendency of the excitations to split into two separated bands is much more pronounced in the final density of states in Fig. 2 than in the RPA.

Some of the parameters in the present calculations differ from those used in the previous MF model. Including δU given by (2.21) in the calculation of the paramagnetic heat capacity, the fit to the experimental position of the maximum in the Schottky anomaly is improved by a slight reduction of the zero-field value of Δ from 0.71 to

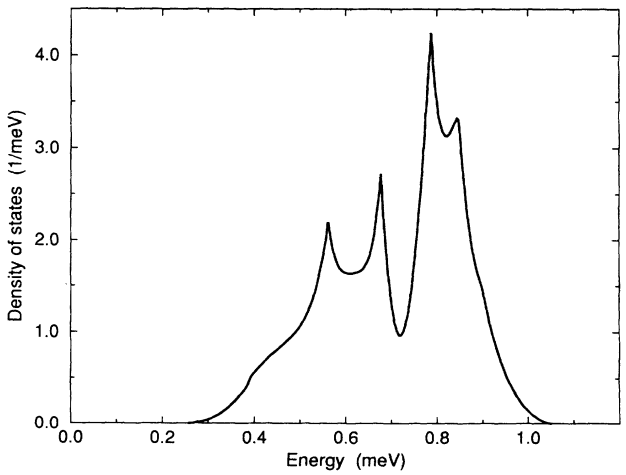

FIG. 2. The final calculated density of states per Ho ion in the low-temperature limit of the paramagnetic phase, $\mathcal{N}(\varepsilon)$. The square-root singularities at the minimum and maximum energies are modified by the directional dependence of the long-wavelength A_1 mode (see Fig. 3).

0.69 meV. This change is accomplished by using

$$V_{60}=-3.42\times10^{-5}\ \text{meV}\ ,$$
$$V_{62}=(6.41-i4.59)\times10^{-5}\ \text{meV}\ , \tag{3.2}$$

whereas the remaining crystal-field parameters are the same as in Table I in Ref. 1. The change also influences weakly the matrix element ($M=6.551$ instead of 6.541). The quality of the fit to the experimental heat capacity is much improved in comparison with the one derived in the MF approximation, as shown in Fig. 4. The fit is now close to perfect below 7 K, where the phonons are unimportant, and down to about 1 K, where critical fluctuations may start to be of importance.

The dominant part of the two-ion coupling, due to the classical dipole-dipole interaction, is unchanged. Given the positions of the magnetic Ho-ions, the dipole-dipole interaction is calculated by the Ewald method utilizing the refinements developed by Bowden and Clark.[12] In order to get agreement with the observed transition temperature, and to explain the larger splitting between the A_1^* and A_2 excitation modes at (100) than that predicted by

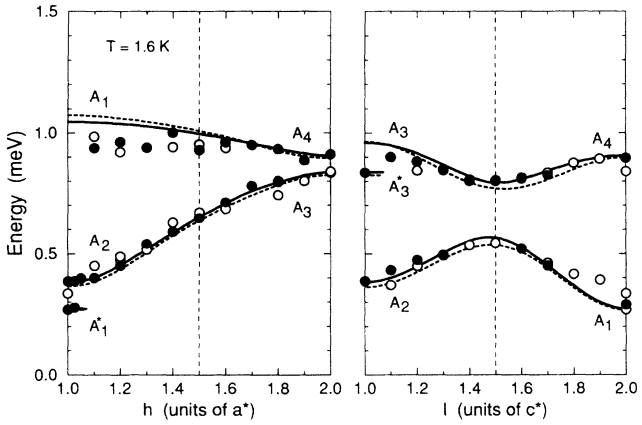

FIG. 3. The dispersion relation of the singlet-singlet excitations along $\mathbf{a}^*$ and $\mathbf{c}^*$ in the paramagnetic phase of HoF_3 at 1.6 K. The closed circles are the experimental results (Ref. 1) obtained with the neutron-scattering vector along (h00) and (00l), whereas the open circles are the results obtained along the energetically-equivalent directions (h01) and (10l) (with h and l lying between 0 and 1). The results are shown in a double zone representation, and the thin dashed lines indicate the Brillouin-zone boundaries. The solid lines are the theoretical predictions including the single-site fluctuations, and the thick dashed lines are the RPA results derived from the MF model in Ref. 1. The labeling of the different modes, A_1-A_4, close to the Bragg points is explained in Ref. 1. The short solid lines marked A_1^* and A_3^* show the energies of the two ferromagnetic modes in the long-wavelength limit, when the direction of the wave vector is perpendicular to, respectively, (h00) and (00l). In combination with the nonzero experimental resolution width, the A_1^* mode in particular contributes much more strongly to the scattering cross section than the A_1 mode close to (100). Resolution effects combined with the singular behavior of the long-wavelength A_1 mode may also be important for explaining the difference between the theoretical and experimental energy of this mode.

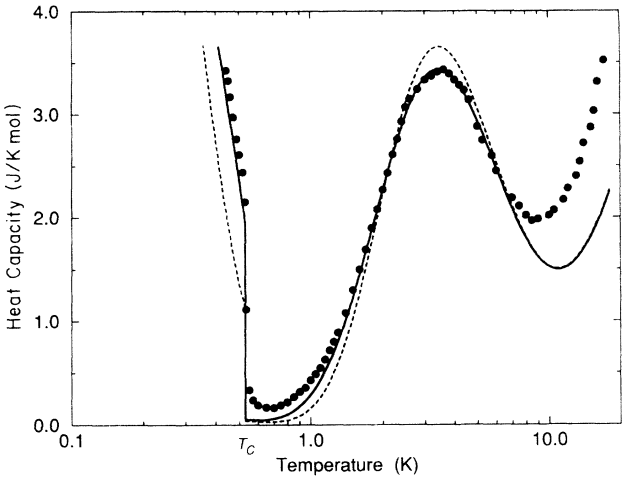

FIG. 4. The low-temperature heat capacity of HoF_3. The solid circles are the experimental results obtained by Bleaney *et al.* (Ref. 3), the dashed line is the magnetic contribution predicted by the MF theory (Ref. 1), and the solid line is the result derived in the present approximation including the effect of the single-site fluctuations. Above 7–8 K the phonons start to contribute, as do the higher-lying $4f$ levels on the Ho ions.

the classical coupling, two exchange-coupling constants, $\mathcal{J}_{13}$ and $\mathcal{J}_{12}$, were used as fitting parameters. They are the isotropic couplings between, respectively, nearest and next-nearest neighbors. To these we here add one more coupling, $\mathcal{J}_{11}$, which is the nearest-neighbor coupling between ions on the same sublattice (the distance between these ions is not much greater than the smallest one). The final values of the three parameters are

$$\mathcal{J}_{13}=-0.30\ \mu\text{eV}\ \ (-0.64\ \mu\text{eV})\ ,$$
$$\mathcal{J}_{12}=0.37\ \mu\text{eV}\ \ (0.30\ \mu\text{eV})\ , \tag{3.3}$$
$$\mathcal{J}_{11}=0.12\ \mu\text{eV}\ \ (0)\ ,$$

where the numbers in the parentheses are the previous values used in the MF model (when $\theta=+25°$). The introduction of the coupling parameter $\mathcal{J}_{11}$ leads here to a slight improvement of the fit to the excitation energies, and thus probably also to a better estimate of the density of states, but it is in no way essential for the analysis. For instance, the reduction of the calculated energy of the upper A_1 mode close to (100) is a pure renormalization effect. The new values of the exchange parameters mean that the effective coupling parameter determining T_c (see Ref. 1).

$$\mathcal{J}_1(\theta)=2\mathcal{J}_{13}\cos2\theta+2\mathcal{J}_{12}+2J_{11}+16.848\mathcal{J}_D \tag{3.4}$$

is now 7.92 μeV, which is about 11% larger than in the MF model. This increase is required in order to compensate for the reduction, by the factor $1+\Sigma(0)$, of the effective single-site susceptibility deriving from the fluctuations. This factor is calculated to be 1.128 just above T_c.

In the calculation of the zero-frequency susceptibility, it is important to include the nuclear contribution due to the hyperfine interaction. This coupling enhances the

susceptibility at T_c by about 16%. To a first approximation the influence of the fluctuations on this coupling may be neglected. However, it is practicable to include the effects of the singlet-singlet fluctuations on the hyperfine coupling, leaving out the intrinsic $1/z$ modification of the nuclear susceptibility (which is of the order A^4). In this approximation the xx component of the effective noninteracting susceptibility, $\tilde{\chi}^o=\chi^o/[1+\Sigma(0)]$, is replaced by

$$\tilde{\chi}^o_{\text{eff}}=\tilde{\chi}^o(1+A^2\tilde{\chi}^o\chi_I) \tag{3.5}$$

and $K(0)$ by approximately $K(0)(1+A^2\tilde{\chi}^o\chi_I)$. $I=\frac{7}{2}$ is the nuclear spin, $A=3.36$ μeV is the hyperfine coupling and χ_I is the nuclear xx susceptibility component as determined from $\mathcal{H}_{\text{hf}}$(eff) given by (3) in Ref. 1. $\bar{\bar{\chi}}^o$ in this Hamiltonian is replaced by $(1/N)\sum_{\mathbf{q}}\bar{\bar{\chi}}(\mathbf{q})$, but this change can be neglected in the quadrupole term.

The maximum value of the renormalization factor, $1+\Sigma(0)$, is 1.140 at $T\simeq 2$ K. Above this temperature $\Sigma(0)$ steadily decreases, and the renormalization is reduced to 1.098 at 4.2 K. The rather weak variation of the renormalization in this temperature interval means that the result for the renormalized temperature-dependent bulk susceptibility in the paramagnetic phase is close to the previous MF-result shown in Fig. 7 in Ref. 1. In the presence of a magnetic field, or in the ordered phase, the mean field is determined by (2.33). The change of this field, δH, induced by the fluctuations, and the moments themselves are calculated fully self-consistently. Above T_c in the low-field limit $\delta H/H_{\text{MF}}=\Sigma(0)$. At higher fields, δH goes through a maximum and then starts to decrease. At low temperatures the maximum value is about 0.3 kOe, and the maximum occurs when the moment is about half its saturation value ($H_{\text{MF}}\simeq 4$ kOe). In the high-field limit $\delta H/H_{\text{MF}}$ vanishes, whereas δH itself becomes small but not zero. It is uncertain whether this is due to the approximations made or not, but the nonzero value of δH at infinite fields has no consequences. More importantly, the area determined by δH as a function of $g\mu_B\langle J_x\rangle$ is found to agree quite accurately with the calculated energy change of the nonmagnetic state induced by the fluctuations. In the low-temperature limit $\delta U/N=-9.06$ μeV and (2.34) is satisfied to within 2–3 %. Only in the high-temperature limit is the integral in (2.34) calculated to vanish somewhat faster than $\delta F(m=0)$, indicating that the elastic contributions should be included in a more careful manner in this limit.

At low fields the calculated renormalized magnetization is close to that predicted by the MF model, corresponding to the behavior of the (zero-field) susceptibility. When the field is applied along the a direction, the magnetization increases very rapidly and is close to its saturation value already at a field of about 10 kOe. At this field the $1/z$ renormalization is nearly quenched, corresponding effectively to an enhancement of the coupling constant. The calculated magnetization at low temperatures and intermediate fields is therefore increased in comparison with the result derived from the MF model. At 4.2 K, when the field is applied along the c axis, the (change of the) renormalization effect is small. In the other case, when the field is along the a axis at 1.6 K, the magnetization is calculated to be somewhat larger than predicted by the MF model, and thus closer to the experimental behavior, as shown in Fig. 5. The figure only contains the results below 25 kOe. The magnetization curves have been measured up to a field of 80 kOe. At the higher fields the results of the two models coincide and are in good agreement with experiment (see Fig. 6 in Ref. 1). The rapid quenching of the fluctuations produced by a field along the a axis at low temperatures is also illustrated by Fig. 6, showing the field dependence of the excitations observed at (001) at 1.6 K. The width of the excitation band, which is close to the distance between the upper and lower excitation in this figure, is reduced by a factor of 5 at 10 kOe, compared to its zero-field value. Above about 25 kOe the excitation band is almost completely flat and the single-site fluctuations are of no importance. The change of the bare interaction parameters means that the present model reproduces the experimental behavior somewhat more accurately than the previous model.

Just above T_c, the entropy due to the electronic singlet-singlet states is vanishingly small, and the heat capacity in the ferrimagnetic phase is determined by the variation in the population of the nuclear levels as in the MF case [thus the calculation of the heat capacity in the ordered phase does not rely on the relation (2.34)]. The effects of the single-site fluctuations are included via the reduction of the mean field derived from (2.33). The result is compared with the experimental data in Fig. 4 showing that the present model, in contrast to the MF model, can almost account for the large jump in the heat capacity observed experimentally at T_c. The improved description of the heat capacity in the ordered phase is related directly to the fact that the ordered moment predicted in the zero-temperature limit is closer to the observed value. As shown in Fig. 7, the discrepancy is re-

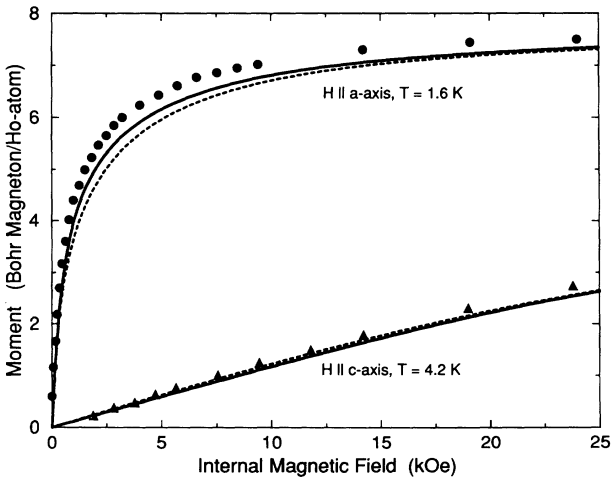

FIG. 5. The magnetic moment of HoF_3 as a function of field along the a axis at 1.6 K and along the c axis at 4.2 K. The experimental results of Bleaney *et al.* (Ref. 3) have been corrected for the demagnetization field estimated from the shape of the samples. The mean-field predictions (Ref. 1) are shown by the dashed lines, and the present calculations by the solid lines.

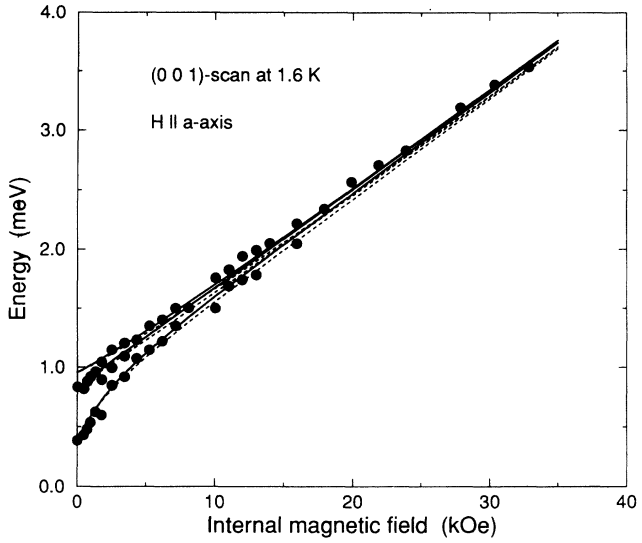

FIG. 6. The position of the inelastic scattering peaks at (001) as a function of magnetic field applied along the a direction at 1.6 K. The circles are the experimental results (Ref. 1) and the dashed and solid lines show the calculated energies of the A_2, A_3^*, and A_3 modes, respectively, in the RPA (Ref. 1) and when including the $1/z$ renormalization. The A_2 and A_3 modes are near the minimum and maximum excitation energies, and the decreasing distance between the upper and lower lines indicates that the total excitation bandwidth rapidly declines as the field is increased.

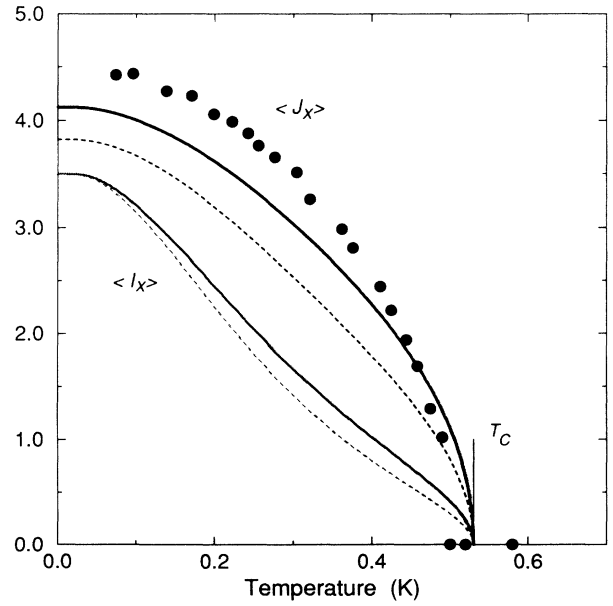

FIG. 7. The solid lines show the calculated values of the angular moment, $\langle J_x \rangle$, and the nuclear spin, $\langle I_x \rangle$, of a Ho ion as a function of temperature below T_c. The dashed lines are the corresponding results derived in the MF case.[1] The filled circles are the experimental values of $\langle J_x \rangle$ determined from the variation of the magnetic scattering intensities at (100) obtained by Brown *et al.* (Ref. 2). Their results have been scaled to agree with the magnetic moment of $5.7\mu_B$, which they obtained from structure refinements at 70 mK.

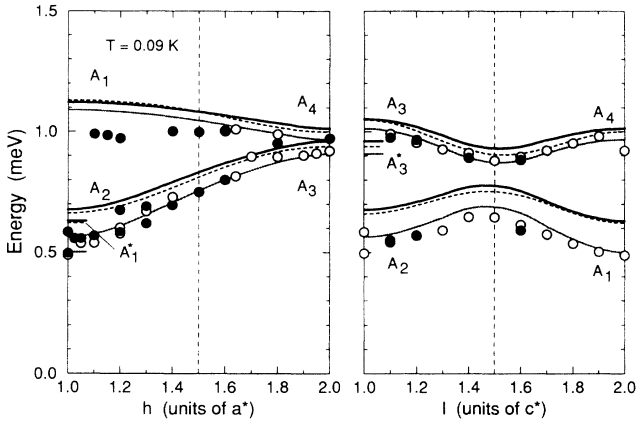

FIG. 8. The dispersion relation along $\mathbf{a}^*$ and $\mathbf{c}^*$ in the ordered phase of HoF_3 at 90 mK. The meaning of the symbols is the same as in Fig. 3. The cross hatched lines show the theoretical results at 0.25 K.

duced by almost a factor of 2, and the calculated moment at $T=0$ is now about 9% instead of 16% smaller than that determined[2] by the neutron-diffraction experiment. The larger value of the ordered moments implies an increase in the excitation energies and, as shown in Fig. 8, the calculated excitation energies at 0.09 K are slightly above those derived from the MF model. It is argued in Ref. 1 that the sample temperature at which the experimental results shown in Fig. 8 were obtained might have been higher than indicated, because of the very large nuclear heat capacity at these temperatures. Here we find that we get a reasonable agreement between theory and experiment, if the sample temperature is assumed to be about 0.25 K.

IV. DISCUSSION AND CONCLUSION

The renormalization effects due to single-site fluctuations have been included to leading order in the case of the singlet-singlet system HoF_3. The expansion of the Matsubara Green function, applicable to this system, is considered to first order in $1/z$. In this order all the single sites are assumed to be placed in equivalent surroundings. The fluctuations in this effective medium, which derive self-consistently from the response of the single sites, affect the single-site Green function in a manner which may be determined by a cumulant expansion. An examination of the cumulants in the series of the single-site Green function shows that the usual "unconditional" $1/z$ expansion could be improved substantially in a straightforward way. One additional advantage of the present procedure is that it is fully self-consistent, and the results therefore also behave properly close to a second-order phase transition.

HoF_3 is almost the ideal system for studying the effects of fluctuations. The electronic properties are nearly determined by the two lowest singlets alone at low temperatures, and the classical dipole-dipole coupling is a factor of 10 larger than other dipole couplings in the system. The single-site properties are simple and the most important part of the two-ion interactions may be calcu-

lated directly. Furthermore, the long-range critical fluctuations close to the phase transition are expected to be of marginal importance, as they only lead to logarithmic corrections to the mean-field behavior. The effects of the $1/z$ fluctuations are calculated to be rather substantial in this system. For instance, the single-site susceptibility is found to be reduced effectively up to 12% at the lowest temperature. In the comparison with the result to the MF model in Ref. 1, these differences are not always manifest, because the renormalization effects to some extent are included in this model via an effective adjustment of the interaction parameters. The renormalization effects vary slowly with temperature but may be quenched rather rapidly by applying a magnetic field, in which case differences may appear between the two models, since the bare interaction parameters are different.

The comparison between theory and experiment has been improved systematically by the inclusion of the effects due to the single-site fluctuations. The most striking improvement is found in the case of the heat capacity. Even so, the experimental heat capacity does not approach zero as closely as the theoretical prediction at temperatures just above T_c, indicating that the critical fluctuations are of some importance, or alternatively that effects of the order $(1/z)^2$ should be included at the lowest temperatures. Although the theoretical magnetization curves, as a function of field or of temperature below T_c, are in better agreement with experiments than found in the MF model, there are still some discrepancies. We do not expect that higher-order renormalization effects can eliminate these deviations. An estimate of the bare electrostatic interaction between the quadrupole moments of the $4f$ electrons on the different ions indicates that this coupling may be of some importance. However, this interaction is expected to be strongly shielded by the other electrons on the Ho and the Cl ions, and the good account of the heat capacity does not leave much room for any additional couplings. The discrepancies are systematic, but they are approaching a level where experimental uncertainties may be significant for the comparisons. Utilizing the correlation between the jump in the heat capacity at T_c and the zero-temperature moment, the comparison of experiment with theory suggests that this moment should be only a few percent larger than calculated, between $5.2-5.4\mu_B$, to be compared with the neutron diffraction result[2] of $5.7\mu_B \pm 0.2\mu_B$. It is therefore apparent that a further refinement of the theoretical understanding of this unique magnetic system must depend on the performance of even more precise experiments.

ACKNOWLEDGMENT

The author would like to thank A. R. Mackintosh for a number of useful comments.

[1]M. J. M. Leask, M. R. Wells, R. C. C. Ward, S. M. Hayden, and J. Jensen, J. Phys. Condens. Matter **6**, 505 (1994).

[2]P. J. Brown, J. B. Forsyth, P. C. Hansen, M. J. M. Leask, R. C. C. Ward, and M. R. Wells, J. Phys. Condens. Matter **2**, 4471 (1990).

[3]B. Bleaney, J. F. Gregg, R. W. Hill, M. Lazzouni, M. J. M. Leask, and M. R. Wells, J. Phys. C **21**, 2721 (1988).

[4]K. K. Sharma, F. H. Spedding, and D. R. Blinde, Phys. Rev. B **24**, 82 (1981); K. Ram and K. K. Sharma, J. Phys. C **18**, 619 (1985).

[5]J. Jensen, J. Phys. C **17**, 5367 (1984).

[6]R. B. Stinchcombe, J. Phys. C **6**, 2459 (1973).

[7]D. H.-Y. Yang and Y.-L. Wang, Phys. Rev. B **10**, 4714 (1974).

[8]C. M. Care and J. W. Tucker, J. Phys. C **10**, 2773 (1977).

[9]Y. Galili and V. Zevin, J. Phys. C **20**, 2543 (1987).

[10]J. Jensen and A. R. Mackintosh, *Rare Earth Magnetism: Structures and Excitations* (Oxford University Press, Oxford, 1991).

[11]J. Jensen, K. A. McEwen, and W. G. Stirling, Phys. Rev. B **35**, 3327 (1987).

[12]G. J. Bowden and R. G. Clark, J. Phys. C **14**, L827 (1981).